SERP+ M2 INTERNSHIP REPORT

Thermal treatments of detonation nanodiamonds: from surface chemistry to colloidal stability

Author: Teodor Jianu

Supervisors: Hugues Girard and Jean-Charles Arnault

Nanodiamonds group, LEDNA laboratory, CEA – Saclay

Page left intentionally blank

TABLE OF CONTENTS

Abstract 4

Acknowledgements 5

List of abbreviations 6

1. Introduction: context and state of the art 7
2. Experimental part: materials, sample preparation and methods 9
3. Results 11
    - 3.1 Characterization of As Received particles. 11
        - 3.2 DNDs annealed from 200°c to 800°c under different vacuum levels (10^{-1} /Z10^{-5} mbar) 15
            - 3.2.1 Evolution of the surface chemistry 15
            - 3.2.2 Colloidal properties of annealed DNDs 17
            - 3.2.3 Annealing treatments of DNDs under hydrogen 18
    - 3.3 DNDs annealed from 900°C to 1100°C 20
    - 3.4 Ionic species generated during sonication under different atmospheres 22
4. Discussion 24
    - 4.1 Surface chemistry modifications and the effect on colloidal behavior 25
    - 4.2 Healing of defects 28
    - 4.3 Graphitization kinetics 28
5. Conclusion and perspectives 29

References 30

Abstract

The current study focuses on the effect of thermal treatments applied on detonation nanodiamonds (DNDs). The temperature range varied between 200°C and 1100°C. FTIR and XPS techniques were employed to investigate the surface chemistry, while DLS, ζ-potential and concentration measurements were involved in assessing the colloidal behavior. Between 200°C and 800°C a reduction of the carboxyl groups was observed with the concomitant formation of the C-H bonds at the surface of the NDs. between 500°C and 900°C degrees, stable colloidal systems were formed. Between 900°C and 1100°C the graphitization of the surface and the effect of annealing time were studied using XRD complementary to the IR and XPS methods. A high content of sp^2-hybridized carbon (> 60%) was quantified for the 1100°C treatments, independent of the annealing times.

Résumé

L'étude actuelle est concentré sur l'effet des traitements thermiques appliqués sur les nanodiamants de détonation (DND). La gamme de température variait entre 200°C et 1100°C. Les techniques FTIR et XPS ont été employées pour étudier la chimie de surface, tandis que la DLS, le potentiel ζ et les mesures de concentration ont été utilisés pour évaluer le comportement colloïdal. Entre 200°C et 800°C, une réduction des groupes carboxyles a été observée avec la formation concomitante de liaisons C-H à la surface des NDs. Entre 500°C et 90°C, des systèmes colloïdaux stables ont été formés. Entre 900°C et 1100°C, la graphitisation de la surface et l'effet du temps de recuit ont été étudiés en utilisant la XRD en complément des méthodes IR et XPS. Un contenu élevé de carbone hybridé sp^2 (> 60%) a été quantifié pour les traitements à 1100°C, indépendamment des temps de recuit.

ACKNOWLEDGEMENTS

To begin with, I want to thank my two supervisors, Hugues Girard and Jean-Charles Arnault, for the great experience they created for my internship. The guidance inside the laboratory, the introduction to the field of nanodiamonds, and the solid explanations are some of the aspects that made my stay at LEDNA a fruitful and pleasant research experience. In addition, I would like to thank the Ph.D. students from the nanodiamonds group: Florent, Kamilia, and Lorris for all the help, patience, and the welcoming, relaxed work environment.

Next, I am so grateful for the opportunity to be a SERP+ student and to experience and grow in so many ways, both professionally and personally. Special thanks to the director of the program and coordinator of Université Paris-Saclay, Sandrine Lacombe and the coordinator of Universidade do Porto, Eduardo Marques. In addition, of course, "best regards" to Eva and Kali for all the support, someone can benefit. On a more personal note, I will always remember with a big smile the "bebes" that made these 2 years have such a warm, friendly feeling: Alicja, Andrea, Christian, Diego, Eva, Lorenzo, Marta, Ola, and Yutzil. You will be missed! Nevertheless, I can't forget all the other colleagues from SERP+ program and the beautiful people I met on the way.

Finally, yet importantly, all appreciation to my family and friends back home who enjoyed this adventure with me and proved that distance is just a small detail. How much pride and yet modesty I found to come from such a beautiful background, to explore so many cultures and open my mind impressed by the uniqueness of this world.

LIST OF ABREVIATIONS

As_Rec – as received
At.% - atomic percent
ATR – Attenuated Total Reflectance
C=O – carbonyl
$C_3H_6N_6O_6$ – hexogen – 1,3,5-Trinitroperhydro-1,3,5-triazine
$C_6H_2(NO_2)_3CH_3$ – TNT – 2,4,6-trinitrotoluene
C-O-C – ether
COOH – carboxylic acid
CVD – chemical vapor deposition
DLS – Dynamic Light Scattering
H_2O_2 – hydrogen peroxide
EDA – electron-donor-acceptor
EPR – Electron paramagnetic resonance spectroscopy
FTIR – Fourier Transformed Infrared
DNDs – detonation nanodiamonds
H_2SO_4 – sulphuric acid
HCl – chlorhidirc acid
HNO_2 – nitrous acid
HNO_3 – nitric acid
HPHT – high pressure high temperature
IR – Infrared
NaCl – sodium chloride
NDs – nanodiamonds
NO_2^- – nitrite radical
N-V centers – Nitrogen-Vacancy centers
SiO_2 – silicium oxide
XPS – X-Ray Photoelectron Spectroscopy
XRD - X-Ray Diffraction
ZrO_2 – zirconium oxide

1. INTRODUCTION

The dynamic of the contemporary world and of modern society grants access to unique and high performance technologies aimed at making one's life easier and more efficient. However, the cost of these tremendous advances lays in increased demand and consumption, which directly affects the ways we utilize resources to meet our needs. It is understandable why one of the main issues that require fast and collective action is the need to shift to renewable energies and lower the negative impact that our fast-paced society has on the planet. One way to tackle this challenge is by employing materials as game changers in the energy related domains. Optimized and promising applications of materials for the mentioned scope require a deep, thorough understanding of their characteristics, structure and behavior under external stimuli. These aspects tend to be different for bulk materials compared to their nanoscale counterparts. A class of such matter that is quickly catching the attention of the scientific community are the carbon-based nanomaterials. The main representatives are graphene, carbon nanotubes, carbon quantum dots, fullerenes, carbon onions and nanodiamonds (NDs)[1]. The latter received great attention based on the versatility and the wide range of applications it can provide. From composite materials to drug delivery systems and catalysts, the diamond nanoscale particles are a promising nanomaterial[2, 3, 4]. Numerous approaches for the synthesis of NDs exist such as the high-energy milling of diamond formed by high pressure high temperature (HPHT) or chemical vapour depositon (CVD).

An alternative consists in an environmentally friendly approach based on the synthesis from explosive molecules (TNT ($C_6H_2(NO_2)_3CH_3$) and hexogen ($C_3H_6N_6O_6$), which are rich in carbon and the released energy ensures that the conversion takes place. In a cooled chamber with an inert gas, the detonation generates 4-5 nm particles with up to 75 wt.% of diamond, resulting in detonation nanodiamonds (DNDs). The detonation soot also contains graphitic carbon, 25-85 wt.%. In this industrial suitable method, impurities (1-8% metals and oxides) are removed using liquid oxidants such as HNO_3, a mixture of H_2SO_4 and HNO_3, HNO_3 and H_2O_2 under pressure or HCl. This purification method however counterweights the acceptable environmental impact of the explosion [6].

An eco-friendlier purification is achieved in air or ozone-enriched air. The result of the method includes increased diamond content, up to 95% and uniform surface functionalization with COOH- or COOR-. One issue with the purified NDs is their tendency to aggregate. Several methods were employed in de-aggregation such as milling with ZrO_2 or SiO_2 ceramic microbeads[5], dry milling resulting in 5-20 nm particles[6] or by high-temperature H_2 treatment, 2-4 nm were obtained after more than 10.000 rpm centrifugation[7]. Subsequently, the re-aggregation of the NDs must be controlled and one successful alternative is by ultrasound assisted NaCl solution treatment[8].

From literature, [10, 11, 15] it is known that NDs have a rich surface chemistry that can be modified through numerous methods depending on their applications and that they also contain nitrogen vacancies (N-V) centers responsible for the fluorescence properties or C-H/C-N defects. The N-V centers are most common for the milled NDs than for DNDs. One characteristic of the NDs that differentiates them from other carbon nanomaterials is that the surface functionalization can be done in a versatile manner without altering the properties of the diamond core. Conveniently, carboxylated NDs described above can be treated with hydrogen (annealing or plasma at high temperature) to obtain hydrogenated NDs. The oxygenated functions are then completely removed[9]. Other functionalization approaches include:

- long-alkyl chains NDs can be obtained by esterification with acylchlorides from hydroxyl groups[10];
- the graphitic carbon can be chemically modified to obtain strong C-C bonds between the surface and the functional groups[10];
- C-N, C-O or C-S moieties are obtained if the chemistry is focused on the functional groups[10];
- hydrogenated NDs can be modified to obtain strong C-C bonds between the diamond core and the attached group by diazonium chemistry. Moreover this reaction leads to the C-O-C bond formation with hydroxylated NDs[10].

Regarding the nanodiamond's characterization methods, the most common techniques include Fourier Transformed Infrared Spectroscopy (FTIR), X-ray photoelectron spectroscopy (XPS), electron microscopy. Dynamic Light Scattering (DLS) and zeta (ζ)-potential techniques are used to characterize the colloidal suspensions. FTIR is suitable to analyze the surface chemistry of NDs due to the transparency of their diamond core. This is not the case for metallic nanoparticles (NPs) or other nanocarbons.

Moving on to the context of the present study, the use of NDs in energy-related applications such as photocatalysis requires a better comprehension of the ligh- matter interaction and of their colloidal behavior. This is why in the laboratory, there are two PhD candidates running their projects on the subject. Briefly, Florent Ducrozet is studying DNDs and the overproduction of hydroxyl radical (OH•) and solvated electrons in radiolysis experiments, while Lorris Saoudi focuses on HPHT NDs and their applications in CO_2 reduction under UV irradiation. One parameter that governs the colloidal behavior of NDs and their response to irradiation is the surface chemistry. Until now, different modification of the chemical composition at the surface were achieved by applying different gas phase treatments (air, H_2, vacuum) at elevated temperatures (above 700°C). Hence, a variety of modifications develop: desorption of functional groups, oxidations, reductions, hydrogenation and graphitization depending on the applied treatment. Yet, the modification coming from thermal treatments at lower temperatures is to be explored. In this framework, we took detailed look at the surface chemistry and colloidal behavior of DNDs annealed under vacuum or under H_2 in the range of 200°C – 1100°C. For this scope, I did a parametric study for each temperature under two vacuum pressures 10^{-1} mbar and 10^{-5} mbar and the hydrogenation at atmospheric pressure. Discussion of the modifications of the surface chemistry is based on the systematic FTIR and XPS results, while understanding of the colloidal behavior comes from DLS and -potential measurements. Furthermore, we also looked at the effect that different sonication atmospheres (air, Ar and O_2) have on the colloidal behavior.

2. EXPERIMENTAL PART

MATERIALS

Detonation nanodiamonds powder (DND - 5nmN, carboxylated) purchased from Adámas Nanotechnologies, Raleigh, NC, USA were used without any further purification. Milli Q water 18.2 MΩ.cm was used as dispersing solvent.

SAMPLE PREPARATION

Annealing under vacuum.
Treatments were executed in a tubular furnace of Carbolite Gero company (Sheffield, USA). For each treatment, approximately 150 mg of as received powder were placed in the center of a quartz tube and then introduced in the middle of the furnace. Vacuum inside the tube (10^{-1} mbar) was achieved by connecting the tube to a primary pumping system and maintained during the annealing. The range of temperatures was between 200 - 1100°C with a duration of 4h. For the 800° to 1100° treatments, additional 8h and 12h annealing times were carried out. Note that the uncertainty on T was ± 1.5 °C. Another set of annealing treatments were also done using a secondary vacuum system (10^{-5} mbar). In this case, the pumping system was turned on for 16 hours prior to the start of the annealing. 500° and 700° temperatures were chosen for the modification of the nanoparticles.

Annealing under hydrogen.
Annealing under hydrogen atmosphere (99.9997% purity) was realized with the same equipment as for vacuum pressure. The tube was connected to hydrogen with a 50 sccm flux. Hydrogenation was executed for 4 hours for the range of 400°C-800°C annealing treatments at atmospheric pressure with a flow of 50 sccm.

SUSPENSIONS PREPARATION

After annealing, the final masses were included between 60-80 mg corresponding to 50-80% recovered material. Then, 20 mg of powder were placed in a 15mL falcon to which 3mL of MiliQ water were added. Respective suspensions and homogenization were obtained using a sonication step of 30 min with a 1s on/off at 60% amplitude and a constant temperature of 10°C (Cup Horn Bioblock Scientific 750W, equipped with a cooling system, Illkirch-Graffenstaden, France). Lastly, a centrifugation step was involved to separate the colloids and the sediment at 2400G for 40 minutes. The supernatants were collected for further analysis. The effect of the chemical atmosphere during sonication was tested by bubbling Argon or Oxygen gas for 30 min in the volume of water prior to the sonication step and inside the falcon during sonication.

FTIR in Attenuated Total Reflectance (ATR) mode.
Infrared spectra were recorded with a Bruker Vertex 70 spectrometer equipped with a diamond ATR system (Billerica, MA, USA). A measure of 2 µL of DND in water were deposited and dried on the ATR crystal (MIRacle, PIKE Technologies, Fitchburg, WI, USA) under N_2 atmosphere (purging flow of 7L/min) before analysis. Acquisitions represent the average of 64 scans recorded with a 4 cm^{-1} resolution at room temperature with a nitrogen-cooled MCT detector.

X-ray Photoelectron Spectroscopy (XPS)

XPS measurements were performed on a Kratos Analytical Axis Ultra DLD spectrometer equipped with a monochromatic Al Kα (1486.6 eV) X-ray source and a charge compensation system (Manchester, UK). The take-off angle was set at 90° relative to the sample surface. Spectra were acquired at a pass energy of 160 eV for the survey, 40 eV for core levels (O 1s, N 1s, C 1s, Zr 3d). C1s spectra shown in this study were acquired at 10 eV to reach a higher energy resolution. Binding energies were referenced to the Au $4f_{7/2}$ peak located at 84 eV. After the background subtraction by a Shirley correction, a curve fitting procedure was carried out to extract the components of the C1s core level using Voigt functions with a Lorentzian to Gaussian ratio of 30%. For the component of sp^2 carbon, an asymmetry factor was added.

X-ray Diffraction (XRD)

The diffraction spectra were recorded using a Bruker-2D-Phaser diffractometer, in the 2θ range 10.012° - 100.12° with a Cu X-ray source (K_α = 1.5406 Å). The XRD analysis was carried out for the 1000°C and 1100°C annealed samples. Around 5 mg of powder were dispersed in acetone and casted onto a silicon wafer. Herein, acetone was preferred to minimize the electrostatic interactions.

Dynamic Light Scattering (DLS) and Zeta Potential Measurements (ζ-potential)

An estimative measurement of the hydrodynamic diameter of the aggregates and the colloidal stability were conducted using a Horiba SZ 100 Partica. All measurements were done for a concentration of 0.5 mg/mL. DLS values were recorded at an angle of 173°.

Final concentrations

Final concentrations of the suspensions were calculated by drying 100µL of the supernatant onto glass slides, which were weighted 3 times prior and after the drop casting using an analytical balance (model origin). The standard error of the weighting was calculated to be around 15%.

3. RESULTS

3.1. CHARACTERIZATION OF AS RECEIVED NANOPARTICLES.

Surface Chemistry of As Received particles

The starting point of the study is the characterization of the surface chemistry, elemental composition, colloidal behavior and approximation of the average hydrodynamic diameter of the untreated particles, herein referred to as “As_rec". The supplier of the DNDs offers a few details about the dark-coloured powders as follows: mean size of independent carboxylated particles is around 5nm with a negative zeta potential. Therefore, preparing a suspension with these particles and using the array of complementary characterization techniques will provide a thorough list of properties.

By employing FTIR, the surface chemistry of DNDs is investigated. Depicted in Figure 1. is the FTIR spectra of these As Received particles. Table 1 shows the corresponding functional groups and the literature reference.

A broad band of high intensity between 1050 cm^{-1} and 1320 cm^{-1} is made of 2 peaks at 1107 cm^{-1} and 1268 cm^{-1} which can be attributed to C-O stretching and bending vibrational modes of several functional groups such as carboxyls, hydroxyls, esters and to C-O-C modes of ethers groups.

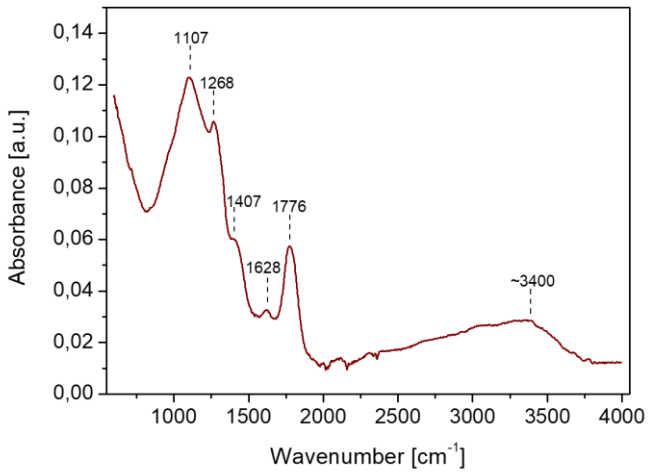

Figure 1.FTIR spectra of As_Rec particles and the wavenumber values of the observed bands.

A discrete shoulder at around 1330 cm^{-1} is attributed to the C-C diamond lattice vibration. Indeed, C-C diamond bonds should be inactive to infrared spectroscopy, but the appearance of this band results from the broken symmetry of the C-C bonds due to high content of nitrogen substitution in the diamond lattice (see XPS). Considering the broad intense bands given by the C-O vibrations that interfere in the same spectral range, this diamond-related peak is not clearly visible due to overlapping. A more obvious shoulder at 1407 cm^{-1} is the signal coming from the symmetric stretching in deprotonated carboxyl groups, while the same vibrational mode of protonated groups is seen as a medium intensity band at 1776 cm^{-1}. In between, a low intensity band at 1628 cm^{-1} comes from the O-H bending of hydroxyls at the surface or from the water molecules. A broad peak at ~3400 cm^{-1} corresponds to the O-H stretching vibration of water adsorbed at the surface of the NDs (bending $\delta(H_2O)$ is present at 1630 cm^{-1} and stretching $\nu(H_2O)$ is located between 3000-3500 cm^{-1} [16]. Despite the fact that the spectrum was recorded under the N_2 gas flow, a clear discrimination between the origin of the O-H is difficult to make as water molecules can still be tightly or loosely bound to the NDs surface [17].

Table 1. Assignment of bands observed in the FTIR spectra of NDs

Wavenumber value/ absorbance frequency [cm^{-1}]	Assigned functional group	Literature value [cm^{-1}]
	C-O stretching, hydroxyl and ether	1050-1150
1100	C-O-C asymmetric bending, ether, ester, lactone; acid anhydride	1100-1140
	C-O stretching, hydroxyl	1090-1140
1268	C-O bending, epoxy, ester	1254-1270
1407	C=O symmetric stretching, deprotonated COOH	1320-1370, 1410
1628	O-H bending, hydroxyl or water	1620-1640 1630 for water
1776	C=O stretching, protonated COOH	1730-1820
3400	O-H stretching, hydroxyl	3300-3500

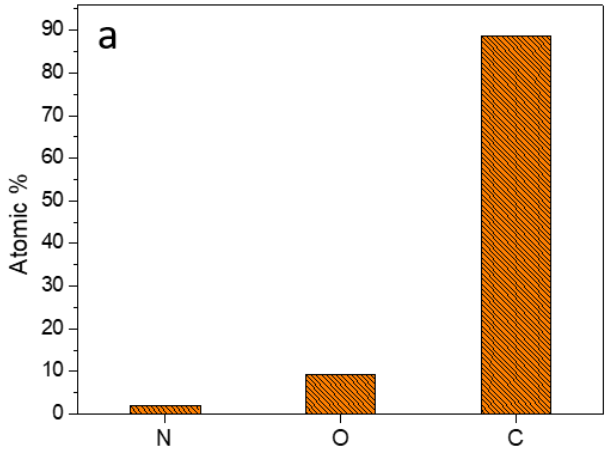

Figure 2.XPS values for the As_Rec particles: a) atomic % of elemental composition,

By XPS analysis it was found that the oxygen content of the As_Rec sample is 9.3 atomic percent (at. %) while the carbon content is 88,8 at.% with the remaining 1,9% being nitrogen (Figure 2). In addition, the C1s core level was fitted with several components (see Figure 3) giving: 3.2% of sp^2 hybridized C-C, 6% sp^3 C-C, 52,8% C-N and disordered sp^3 C-C, 31.1 % C-O and 6.1% C=O and COOH (Figure 3b). The low amount of sp^3 C-C may be surprising, however it is well documented [18, 19] that DNDs are highly defective compared with other classes of NDs, milled from HPHT for example. Here, the diamond core of the particle is mostly represented by the disordered sp^3 C-C component. Despite the fact that quantification of IR absorption spectrum is difficult, by looking at the relative intensity of the band and the XPS values of the corresponding chemical moieties, it can be said that the two methods are complementary and offer both a qualitative and quantitative view on the surface chemistry. Both techniques confirm a high proportion of oxygenated groups at the surface, including COOH.

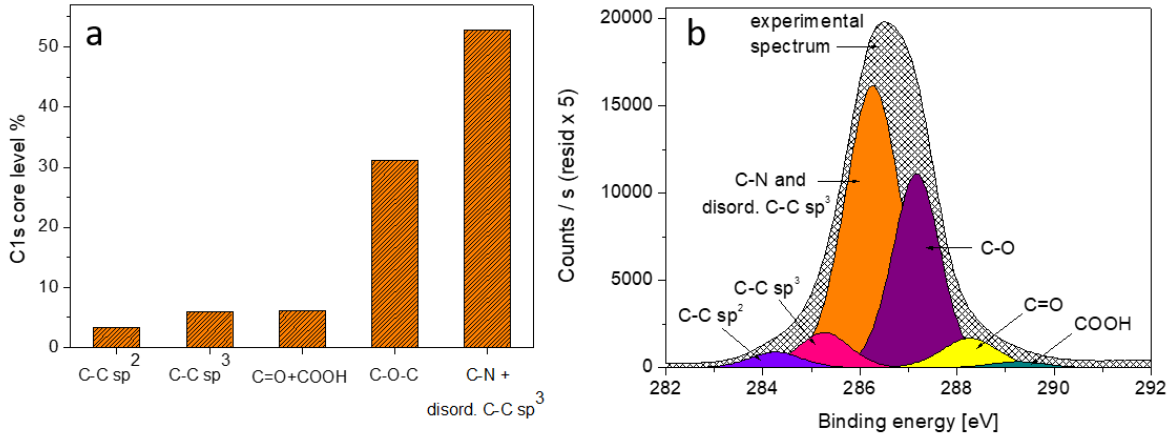

Figure 3. a) Components of the C1s core level as %,
b) Fitting of the C1s experimental spectrum and the areas of the components

Colloidal behavior of As Received particles

When oxidized, NDs have a hydrophilic nature, their dispersion in aqueous media is ensured by the electrostatic repulsions between the COO^- groups at the surface [20]. Yet, their surface affinity for water is not enough to obtain colloidal systems and an external source of energy, herein represented by ultrasound waves, is required to disrupt de Van der Waals bonds between agglomerates and promote hydrogen bonding with the water to form colloids [21, 22]. By measuring the electric potential of the aggregate's double layer, the colloidal stability can be assessed. In the case of As_rec particles at a concentration of 0.5 mg/mL, the obtained ζ-potential is -53 ± 1 mV after 1 day (Figure 4a) and -52 ± 3 mV after 8 days. Generally, the colloidal systems formed by NDs with a ζ-potential value outside the range of [+30,-30] mV are considered to have good colloidal stability, based on the repulsive forces between the charges [23]. Here, the negative ζ-potential can be explained using the surface chemistry, which is rich in carboxyl groups, as previously shown by FTIR and XPS. In water, COOH dissociates into COO^- ions, which negatively charge the double layer around the aggregates. The resulting H^+ ions will interact with water resulting in the formation of hydronium ions (H_3O^+) [23, 24]. A schematic representation of the negatively charged double layer is shown in Figure 4b.

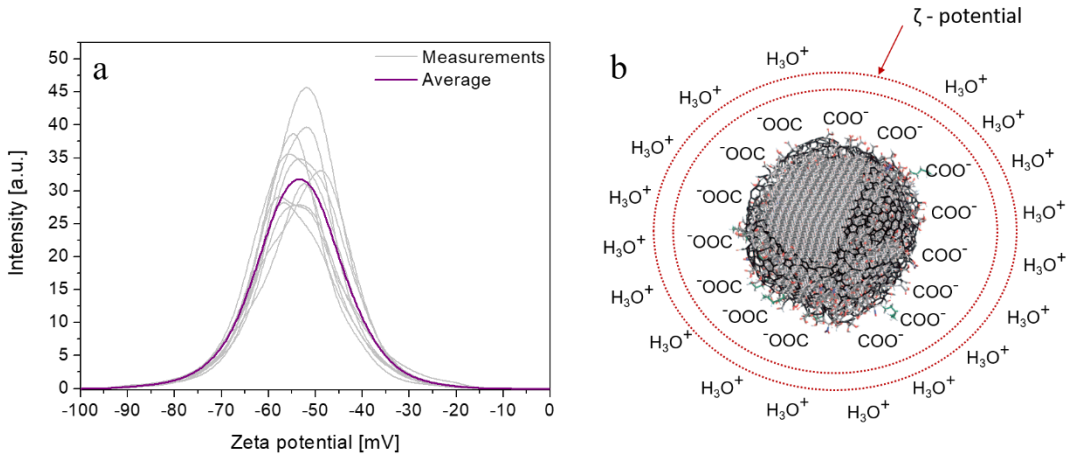

Figure 4. a) Zeta-Potential value for AS_Rec colloidal suspension after 1 day b) scehmatic representation of the negatively charged double layer around the nanodiamond.

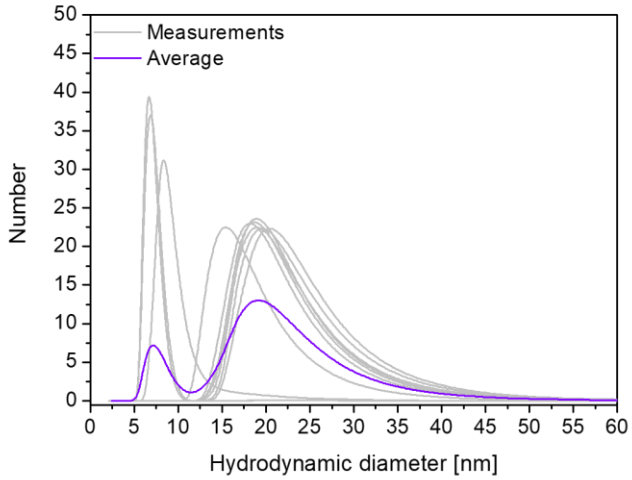

Figure 5. Hydrodynamic diameter of As Received aggregates after 1 day.

The hydrodynamic diameter of the objects in suspension was found to be 37 ± 8 nm using DLS measurements. Figure 5 shows the DLS measurements expressed as distribution of the number of objects of same size. It is clear that the suspension is polydisperse with two main populations having sizes between 5-10 nm and 15-35 nm. The first population represents isolated particles, while the second one stand for small aggregates made of a few particles.

3.2 *DNDs ANNEALED FROM 200°C TO 800°C UNDER TWO DIFFERENT VACUUM PRESSURES (10^{-1} AND 10^{-5} MBAR).*

3.2.1. Evolution of the surface chemistry.

The surface chemistry is subjected to different modifications upon applying thermal treatments. Annealing under vacuum was then applied to these As Received particles, at temperature ranging from 200°C to 800°C. For each temperature, the surface chemistry was investigated by FTIR and XPS. Furthermore, to evaluate the effect of the residual pressure during the treatment, two different systems of pumping were used, reaching 10^{-1} mbar and 10^{-5} mbar vacuum pressures.

For the first set of experiments (10^{-1} mbar) Figure 6 shows the IR spectra of the samples with the respective changes in the surface chemistry. Looking at the oxidized groups bands, at 200°C the C=O band at 1776 cm^{-1} has the same position as for the As Received particles. With increase in temperature both a blue shifting and a decrease in intensity is observed. At 600°C the spectral value of the C=O is 1723 cm^{-1}, this position remaining constant with further increase in temperature. The evolution is related to the reduction of the carboxylic groups, apsect to be discussed. The C-O bands observed between 1270 cm^{-1} and 1090 cm^{-1} are steadily decreasing in intensity with the annealing temperature, reaching a minimum of absorption between 700°C and 800°C. Appearance of C-H symmetric or asymmetric stretching modes are observed between 2830-2960 cm^{-1} [11] starting with 450°C. In this study, weak C-H bands are observed between 2850 cm^{-1} and 2955 cm^{-1} spectral range. In addition, the shape slightly varies for the analyzed samples. This shifting and difference in shape could be explained by a chemical point of view, namely the C-H is part of varying length hydrocarbons (ethyl, propyl or butyl groups) with symmetric or asymmetric stretching modes [25]. From a physical point of view, the C-H containing moieties are grafted onto different facets of the nanodiamond[13] and the orientation and the interactions of these facets with the IR radiation results in slightly different vibrations of C-H stretching.

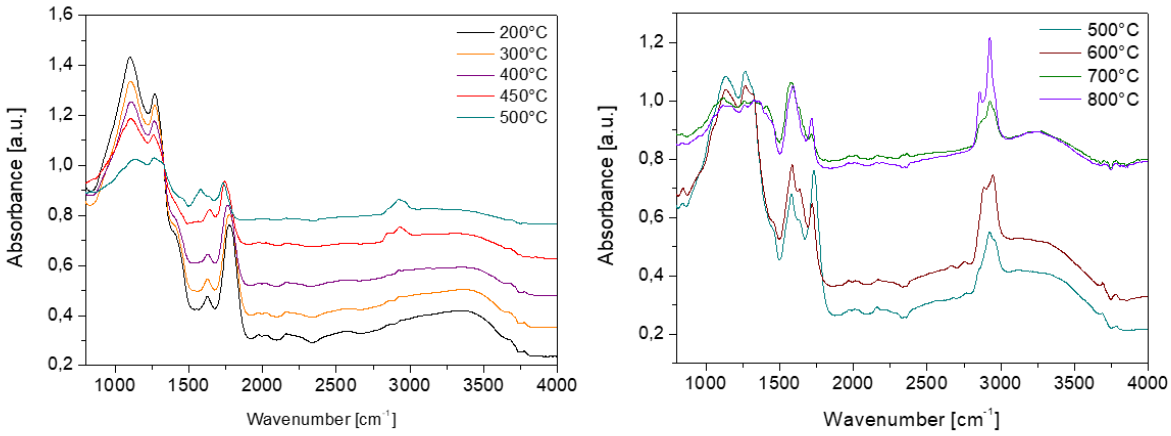

Figure 6. FTIR spectra of annealed DNDs (normalization at 1332cm^{-1}).

By employing a secondary vacuum system (10^{-5} mbar), a better desorption of contaminants, water and H containing groups in the vicinity of the particles prior to applying the thermal treatment is expected. As a comparison, two experiments were done with a pumping system

equipped with a turbomolecular pump: pumping overnight at room temperature and pumping overnight at 200°C. In these experiments, we also added to the protocol a preliminary pumping over the night either at room temperature or at 200°C. The underlying idea was to reduce at its maximum the presence of water residues during the annealing at high temperature. Figure 7 shows the FTIR spectra normalized at 1332 cm^{-1}, corresponding to the diamond peak. This normalization was done to have a better view on the possible relative differences in surface chemistry.

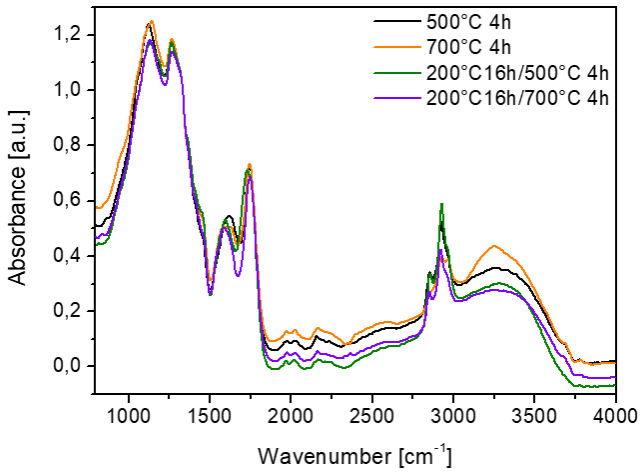

Figure 7. FTIR spectra of particles annealed at 500°C and 700°C under 10^{-5} vacuum pressure with and without thermal treatment overnight (200°C16h)

It can be seen that the pressure values and the thermal pretreatment do not influence considerably the formation of functional groups on the NDs. The C-O-C and C=O bands slightly vary in intensity, while the difference in intensity of the C-H peak follows the same trend as for the 10^{-1} mbar annealing treatments.

To get more insights on the modification induced by the annealing treatments on our NDs, XPS analysis were realized on almost each treated sample. As for As Received sample, deconvolution of the C1s core level has been realized. The evolution of each component according to the annealing temperature is given in Figure 8.

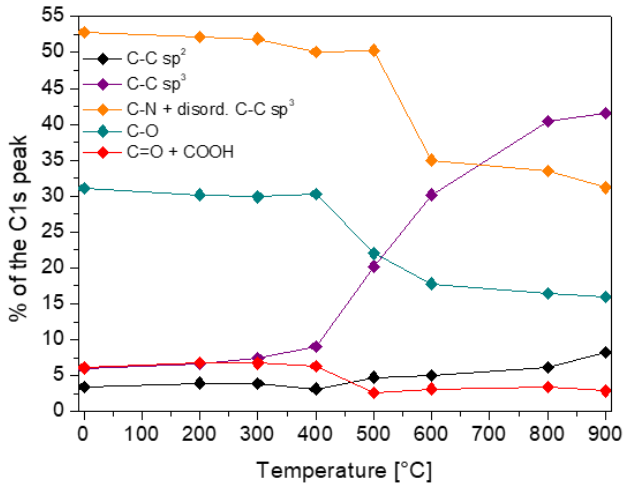

Figure 8. Percentage of components of the C1s peak in the range of 0°C-900°C treatments.

Having a look at the trend specific to each of the C1s core level components, a comprehensive view on the changes occurring during annealing is reached. Looking at the sp^3 C-C component, we can notice a clear increase in its proportion starting with 300°C. From less than 7% on As Received, this component reaches more than 40% of the total C1s core leverl after annealing at 900°C. In the meantime the disorganized C-C sp^3 and C-N components decreases from 50.3 % at 500°C to 35% at 600°C and reaches 31.2% at 900°C, this component being 52.8% in the initial particles. This evolution will be discussed in more detail in the last part of this report. As expected when looking to the FTIR evolution, the C-O content drops from 30.3% at 400°C to 16% at 900°C. In the case of C=O and COOH proportion, no variation is observed in the 0-400°C range, remaining at 6-7% of the total

C1s core level. However, its proportion drops as soon as 500°C is reached, decreasing down to 2.5-3.5%. For the sp^2 C-C component, no evolution is seen until 400°C (less than 4%). Between 500°C and 800°C the proportion remains quite stable, after which, the content of sp^2 C-C reaches 8.3% at 900°C.

3.2.2 Colloidal properties of annealed NDs

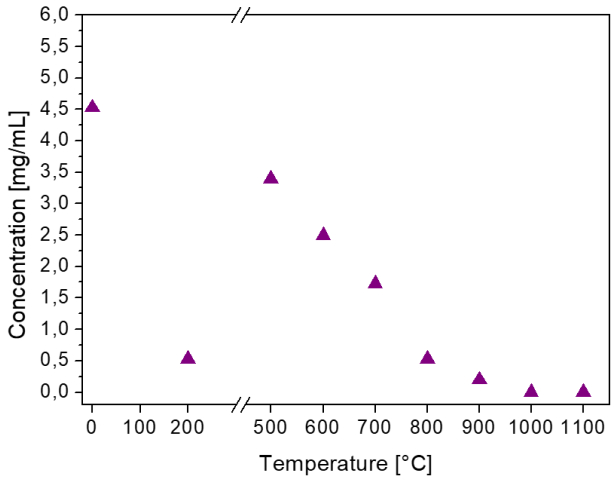

Figure 9. Final concentrations of the suspensions sonicated in different chemical atmospheres

Treated NDs were then suspended in water to evaluate their colloidal behavior. First, we observed differences in the ability of each treated particles to provide a colloidal suspension. This ability can be first evaluated by the concentration in NDs of the supernatents collected after the centrifugation step (see Figure 9). For As Received particles, with our sonication/centrifugation protocol, we measured a concentration of 4.5 mg/mL. A strong decrease is observed for particles treated at 200°C, with only 0.5 mg/mL remaining in the supernatant. For 300°C and 400°C, no particles were collected in the supernatant. Then, at 500°C, part of the particles were once again stable in suspension, with a final concentration of 3.4 mg/mL. However, this value tends to decrease with the raise of the annealing temperature. Figure 10a depicts the ζ-potential values for each sample that could form a colloidal stable system. From a low negative value of -53 mV for the As Received particles, the colloidal stability increases up to -25mV for the samples annealed at 200°C. At 300°C and 400°C, no colloidal stability is reached, however is regained at 500°C. For this sample, the ζ-potential is highly positive (44 mV), meaning that this switch from a negative to a positive ζ-potential is related to a consequent modification of the NDs annealed at 500°C, to be discussed later. The stability is kept constant with the increase in temperature.

Regarding the average size of the aggregates, the mean hydrodynamic diameters are depicted in Figure 10b. In the annealing range of 500-800°C and for the As Received sample, the particles form aggregates of stable mean diameter (50nm and 40nm respectively), while for the 200°C treatment, the value is 3 times higher (168 nm). This tendency of forming larger aggregates can be explained based on the ζ-potential value (-26mV). Having a less charged double layer thus lower colloidal stability, the electrostatic repulsions are not as strong as for other suspensions.

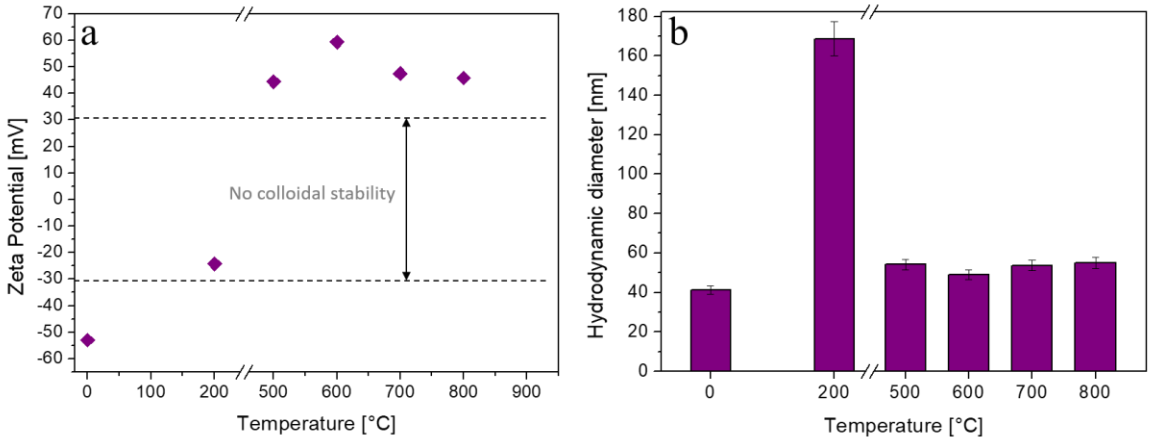

Figure 10. a) Average values of ζ-potential measurements.
b) Average values of hydrodynamic diameter of the aggregates.

3.2.3 Annealing treatments under hydrogen

An important information given by the parametric study presented above on the annealing under vacuum from 200°C to 900°C concerns the appearance of C-H stretching modes between 450°C and 500°C. The question of the origin of this hydrogen has been raised, this is why similar treatment using a better pumping system have been performed. However, these experiments did not give us valuable information on the origin of this hydrogen. Here, we wanted to check if the appearance of these C-H stretching modes occurs at the same temperature when hydrogen is voluntary introduced in the gas phase, and if the shape of the FTIR signature is similar. These experiments were performed between 400°C-800°C under atmospheric pressure of H_2 with a flow of 50 sccm.

Figure 11a. shows the FTIR spectra of samples obtained by annealing treatments done under vacuum and hydrogenation under atmospheric pressure. It is observed that the hydrogen saturated atmosphere does not play a crucial role in the formation of the C-H at the surface of the particles (in terms of shape and spectral range). These C-H bond appears in the FTIR spectra independently of the annealing atmosphere (H_2, primary or secondary vacuum). We can just notice that for the 400°C under H_2, a simple band at 2930cm^{-1} can be observed, thus the formation of the bond seems to be promoted at lower temperature under hydrogen atmosphere.

Concerning the evolution of the oxidized functions, the C=O bands are distinguished at lower wavenumbers after hydrogenation compared to the vacuum annealed samples. The blueshifting of this band occurs in a shorter temperature range, with the minimum in absorbance of the signal at 1710 cm^{-1} noted at 500°C compared to 1723cm-1 at 600°C treatment under vacuum annealing. The C-O band steadily disappears, following the trend as for the vacuum annealed treatments.

As the C-O bands decrease in intensity, the peak at 1332 cm^{-1} can be seen starting with 600°C.

Hydrogenated particles were then suspended in water using exactly the same protocol than for vacuum annealed powders. Concentrations measured in the supernatants are given in Figure 11b. and evidence more concentrated suspension for ND treated under H_2, for the same annealing temperature. Here, one may take into account the better desorption of C=O bonds under H_2 but others parameters may be considered, as it will discussed later.

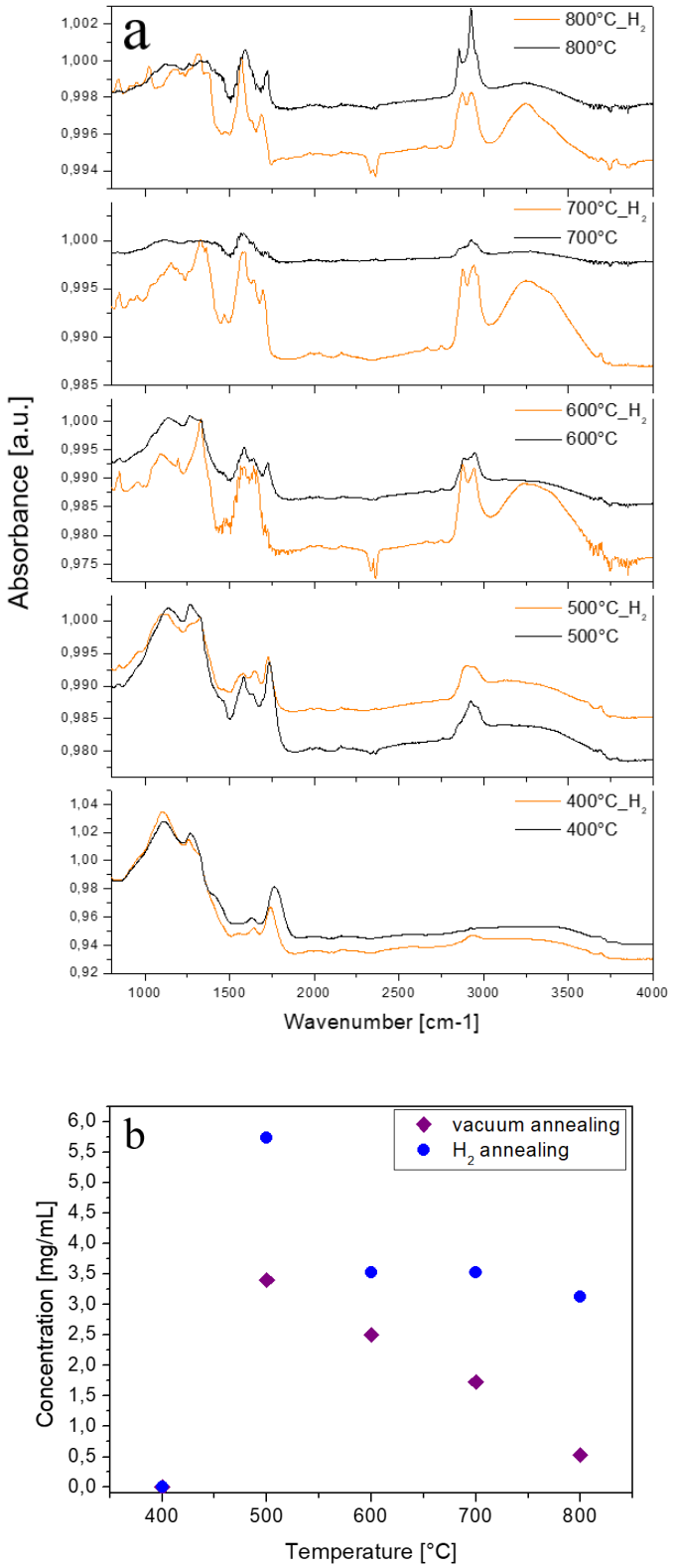

Figure 11. a) FTIR spectra of samples obtained by annealing treatments done under vacuum and hydrogenation under atmospheric pressure
b) Concentrations of suspension obtained by annealing treatments done under vacuum and hydrogenation under atmospheric pressure

3.3 DNDs ANNEALED FROM 900°C TO 1100°C

Literature reports that graphitization of the surface of NDs starts with annealing temperatures above 900°C [26], when the sp^3–hybridized carbon atoms rearrange into a π-conjugated framework that further reorganizes into a graphitic layer covering the diamond core. Then, the graphitization reaches the second outershell and progressively consumes the diamond core. Moreover, the desorption of oxygen-containing groups observed for the 200°C-800°C temperature range leads to the formation of structural defects and dangling bonds which are very likely to promote the transition of sp^3 carbon to sp^2 carbon. Thus, a hybrid sp^2/sp^3 nanostructure is obtained with interesting applications in carbocatalysis [26].

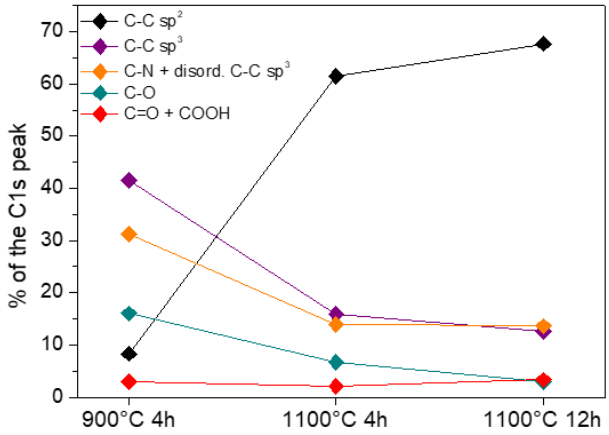

Figure 12. Percentage of components of the C1s peak in the range of 900°C - 1100°C treatments

Herein, the graphitization at three different temperatures, 900°C, 1000°C and 1100°C for three different durations respectively 4, 8 and 12 hours were studied to obtain an initial insight into the kinetics of graphitization. For 1000°C and 1100°C, we were not able to record a spectrum, probably due to the strong IR absorbance of sp^2 carbon. XPS results are depicted in Figure 12. For the sp^2-hybridized carbon component, the trend shows a drastic increase in the percentage from 8.3% for the 900°C 4h sample to more than 60% for the 1100°C annealing experiments. It is very important to mention that in XPS analysis, a 2.5-fold enhancement of the sp^2-hybridized carbon content occurs based on a "nano" effect at the surface of the π-conjugated framework. This effect is addressed for graphitized DNDs [31] and well described elsewhere [27]. Thus, considering this 2.5 enhancement factor for the 1100°C treatments, we can recalculate the sp^2-hybridized carbon content to 24.6% for the 4h annealing time and 27.1% for the 12h one. This proportion of sp^2-hybridized carbon in our treated ND remains remarkable and clearly highlight the consumption of the diamond core into graphite. Consequently, all the others components of the C1s core level decrease (C-C sp^3, defectuous C-C sp^3, C-O) except the C=O bonds which were already minimized.

Concerning the duration of the annealing treatment, it does not induce significant changes in the surface chemical composition, while the temperature plays a noteworthy role on the surface chemistry modifications. These treated particles were also sonicated in water and then centrifuged, however they did not form any suspensions.

Complementary to the XPS technique, XRD analysis is a quick, straightforward method useful to discriminate between the two hybridization states of the carbon. Figure 13 shows the XRD spectra for the 1000°C and 1100°C annealed samples. In the diffraction patterns, the three peaks at approximately $2\theta = 44°$, 76° and 92° corresponding to (111), (220) and (311) reflection planes of diamond lattice can be observed [4,7]. For graphite a single peak at $2\theta = 22°$ appears for all samples annealed at 1100°C. The presence of this peak reveals a crystalline order of sp^2 carbon

not observed for lower annealing temperature, especially 1000°C. However, this diffraction peak remains broad compared to the graphite reference. The broadening of the peaks comes from the nanometric size of the particles.

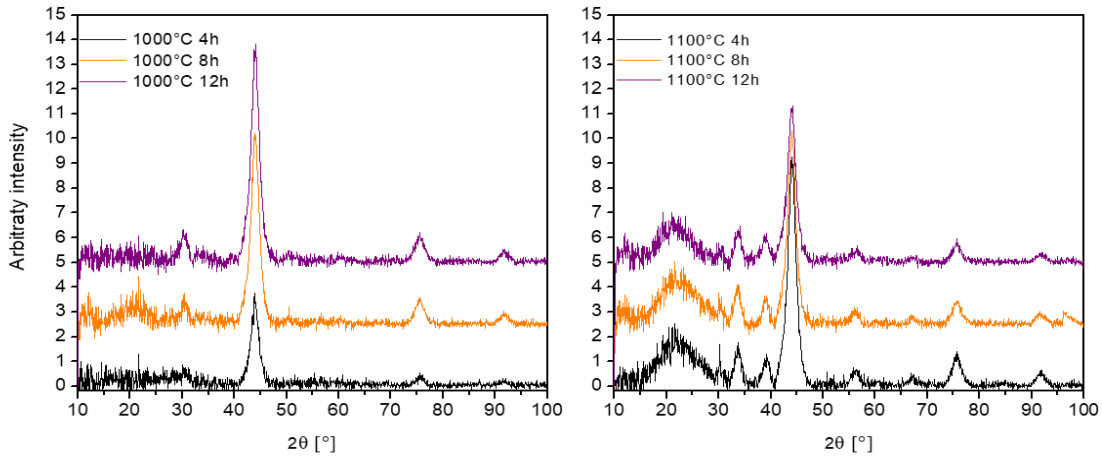

Figure 13. XRD spectra for the 1000°C and 1100°C treatment annealed for different times

The diamond crystalline domain, which can be approximated to the diamond core of the ND, can be calculated using the Scherrer equation:

$$d = \frac{\lambda}{\beta \cos(\theta)}$$

where λ is the X-ray wavelength, β is FWHM and θ is the Bragg angle.

For the untreated particles, the diamond crystallite size was calculated to be 4.7 nm. For the 1000°C and 1100°C annealed samples, the sizes of the crystallites are shown in Table 2 below. The calculated sizes are characteristic to detonation nanodiamonds and in agreement with the specifications provided by the supplier. However, even though the XRD spectra shows the diffraction peak corresponding to graphite, we are not able to detect a diminution of the diamond crystalline domain.

Table 2. Crystallite sizes for samples annealed at 1000°C and 1100°C

	Time		
Temperature	4h	8h	12h
1000C°	4,7 ± 0,8 nm	4,4 ± 0,3 nm	4,3 ± 0,9 nm
1100°C	4,7 ± 0,8 nm	4,7 ± 0,8 nm	4,7 ± 0,5 nm

3.4 IONIC SPECIES GENERATED DURING SONICATION UNDER DIFFERENT ATMOSPHERES

Values for the concentrations of suspensions obtained under different chemical atmospheres clearly show that the highest concentration was obtained for 500°C in all cases, corresponding to 50% of the values for the as received particles. The choice of comparing different atmospheres is done based on the sonochemistry that occurs during the process. N_2 and O_2 gasses dissolved in water can produce N• and O• radicals under the influence of high amplitude shockwaves produced by the cavitation phenomenon [28]. During sonication, bubbles or cavities are formed and their breakage leads to intense heating (up to 5000°C) and high pressures (up to 1000 atm.) for very short times (heating-cooling rate higher than 1010 K/s). In these conditions, HNO_2 and HNO_3 are formed in the gas phase after which dissolve in water and dissociate into ions [29]. Inside the cavitation bubble, several ultrasonic chemical reactions occur. The oxygen atom, O, formed because the presence of O_2 reacts with N_2 gas to form NO• radicals and N• atom. Consequently NO• reacts with O to form NO_2 radicals. The nitrite reacts close to the bubble-liquid interface with hydroxyl radicals coming from the water dissociation to form HNO_2 while NO_2• lead to HNO_3 formation. Reactions 1 to 7 prove the formation mechanism of nitrous acid [30].

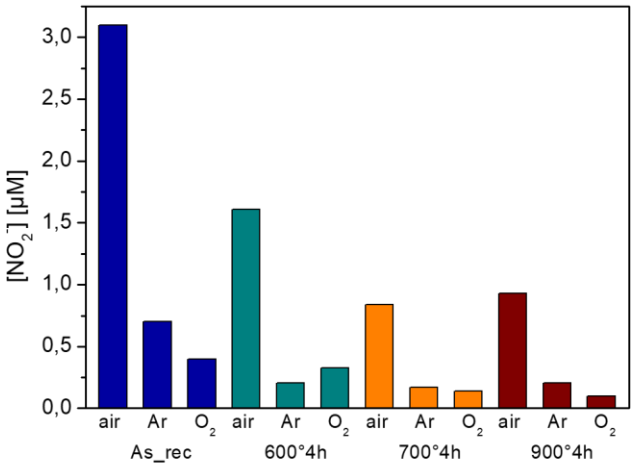

Figure 14. NO_2^- concentrations for different annealing temperatures and different sonication atmospheres.

In the case of this study, the efficiency of the optimized bubbling method was verified by determination of NO_2^- concentration via fluorescence titrimetric method (Figure 14). It was observed that for the As_rec particles the concentration is the highest, while this value decreases with the increase of the annealing temperature. For the samples sonicated in the presence of one of the gasses, in all cases, a sharp decrease in the NO_2^- content is around 80% for Ar and 90% for O_2, respectively (determination done by Florent D. at ICP Paris-Saclay).

$H_2O \rightarrow H\bullet + OH\bullet$ [1]

$O_2 \rightarrow 2O$ [2]

$N2 + O \rightarrow NO\bullet + N\bullet$ [3]

$N\bullet + O \rightarrow NO\bullet$ [4]

$NO\bullet + O \rightarrow NO_2$ [5]

$OH\bullet + NO\bullet \rightarrow HNO_2$ [6]

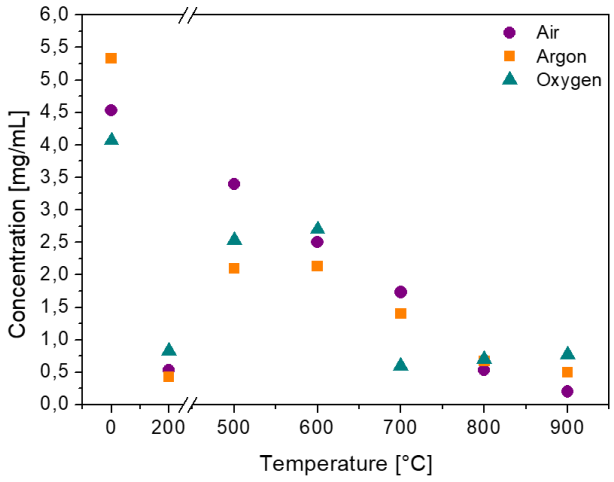

Figure 15. Final concentrations of the suspensions sonicated in different chemical atmospheres

The effect the sonication atmosphere has on the colloidal behavior of the annealed NDs was then analyzed. Recalling the values obtained for the air sonication, the concentrations for the As Received particles are above 4.0 mg/mL for all sonication atmosphere. Between 500°C and 600°C, the highest concentration among the annealing treatment are calculated for all three chemical environments, between 2.0 and 3.0 mg/mL (Figure 15). The hydrodynamic diameter is constant for the particles annealed between 500°C and 900°C, with the mean size of the aggregates being around 50nm. For the same range of temperatures, the suspensions have good colloidal stability with ζ-potential values above 30mV in all cases. The 200°C sample forms bigger aggregates for the oxygen saturated sonication (122 nm) related to the less stable colloidal system (ζ-potential = -27mV). The main observation is that the chemical atmosphere in which the sonication was undergone does not play a crucial role on the colloidal properties of annealed DNDs. All these trends are depicted in Figure 16 below.

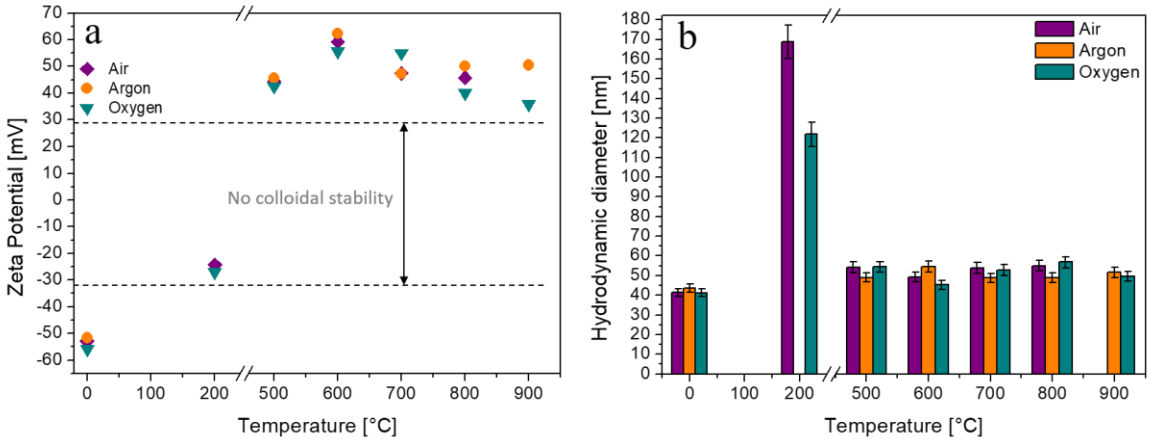

Figure 16. a) Average values of hydrodynamic diameter of the aggregates b) Average values of ζ-potential measurement

4. DISCUSSION

FTIR was employed in detection of functional groups, adsorbed molecules, as well as modifications in the chemistry of functionalized NDs surface. By IR spectroscopy, the different chemical moieties can be identified by the absorption of infrared radiation and the vibrational-rotational modes arising from this absorption. It is worth mentioning that the diamond core is transparent to IR radiation (unless the C-C sp^3 symmetry is broken), therefore this technique is highly sensitive to the surface functional groups. Below, the most important characteristics for NDs of IR spectra are summarized [11]:

Tableau 3. IR spectral range values and respective modes of vibration of functional groups grafted onto the NDs surface

Wavenumber [cm^{-1}]	Chemical bond	Mode of vibration
940	C-O-C	Stretching
1090-1140	C-O	Stretching
1110-1140	C-O-C	Asymmetric bending
1332	C-C	Broken symmetric stretching
1535–1595	C=C	Stretching
1555	C=O	Asymmetric stretching
1650-1858	C=O	Stretching
2850–2855	CH_2	Symmetric stretching
2870-2880	CH_3	Symmetric stretching
2920-2930	CH_2	Asymmetric stretching
2940-2955	CH_3	Asymmetric stretching
3300-3500	O-H	Stretching

XPS is a well-established technique in which the binding energy (E_B) between two atoms is indirectly calculated from the kinetic energy of the photoelectrons leaving the atomic core-shells as a result of interaction with X-ray radiation. For DNDs, which contain diamond carbon, amorphous sp^2 carbon, nitrogen and oxygen atoms, the binding energies between different states of carbon can be used to quantify the atomic percentage of each elemental component. Discrimination between the binding states is based on the shifts in terms of binding energy for different chemical groups. For C-C in the diamond structure, the E_B = 284.5eV [12]. Below, all the energy shifts corresponding to different functional groups are summarized in table 4 [12]. Alongside FTIR spectroscopy, the two techniques are complementary in surface chemistry analysis.

Table 4. Binding energy values of carbon chemical bonds (C1s core level)

Probed chemical bond	Binding energy [eV]
C-C sp^2	283.5
asymmetric C-C sp^2	284.1
C-C sp^3	284.5
Defects (C-N, disordered C-C sp^3)	285.5
C-O	286.4
C=O + COOH	287.5-288.5

Moreover, the interaction of an X-ray beam with the NDs can be useful to obtain an initial idea about the graphitization process at the surface. In the X-Ray Diffraction (XRD) technique, the different planes of the diamond core and the graphitic layer show different diffraction peaks in the resulting spectrum. Usually, sp^3 carbon shows 3 peaks at 2θ = 44.0°, 75.6° and 91.7° corresponding to the (111), (220) and (311) crystallographic planes [4, 7]. For sufficiently crystalline graphite layers, a single peak appears at 2θ = 24° [13].

4.1 SURFACE CHEMISTRY MODIFICATIONS AND THE EFFECT ON COLLOIDAL BEHAVIOR

In literature, the C=O vibration is referred to as having a broad absorption peak between 1720-1780 cm^{-1}. In the spectrum, strong bands can be observed between 1720-1780 cm^{-1} associated with the vibrations of C=O groups of different chemical moieties such as carboxylic acids, esters, lactones, acid anhydrides, etc. [16]. Having a look at these bands, a blueshift (from 1776 cm^{-1} to 1723 cm^{-1}) of the signal occurs with the increase of temperature up to 600° where it completely disappears (see figure 17). This shift can be interpreted as the reduction of the carboxyl moieties to ketones, aldehydes and carbonyls [11]. It is pertinent here to compare these observation to the thermogravimetric analysis (TGA) performed on as received DND particles from the same supplier under inert atmosphere. We observed two main mass drops which were correlated with water desorption between 100°C and 200°C and carbon-oxygen functions removal between 500°C and 700°C [31]. This second peak exactly correspond to the region at which we observe the blueshift of the C=O stretching modes. In a study conducted by [32] on similar DND, it was found that the products of thermal desorption are H_2O (100–600°C), hydrocarbons (200–400°C), CO_2 (200–600°C), CO (400–1000°C), and H_2 (above 800°C). The origin of the CO_2 and CO are the carboxyl groups and hydroxyl groups being removed and thermally degraded in the range of 200°C - 700°C. In the meantime, we observed a switch of the ζ-potential values in this range of temperatures. From still negative at 200°C, it became positive at 500°C. As mentioned previously, COO- coming

from the carboxyl dissociation is at the origin of the negatively charged particles. Here we have a good illustration of the disappearance of this negative charge, with the reduction of the carboxylic acids to aldehydes, ketones and carbonyls, which leaves a surface positively charged.

As already mentioned, the same loss occurs for the C-O groups, confirming the reduction, as well as the desorption processes that occur during vacuum annealing. Comparing the wavenumber values of the C=O bands present for the two treatments, it is seen that lower values are recorded for the hydrogenation treatment. Reduction of C=O bonds occurred more efficiently for the hydrogenation treatment undergone at atmospheric pressure.

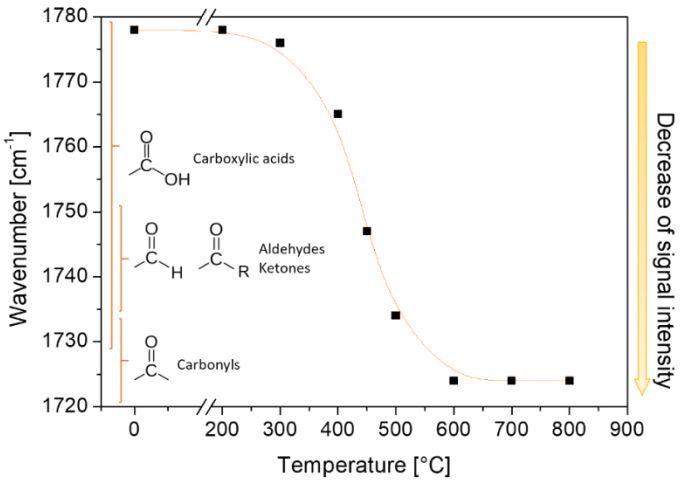

Figure 17. Wavenumber values of C=O bands in the temeprature range 0°C-900°showing the reduction of carboxylic acids at the surface of the NDs

Another aspect to be discussed is the water and O-H containing moieties desorption from the NDs surface. The vibrations modes of O-H correspond to stretching (O-H) at around 3000-3600 cm^{-1} and, in water, bending $\delta(H_2O)$ at 1630 cm^{-1} [16]. In the current spectra the (O-H) mode is seen as a broad band with highest absorbance intensity at 3400 cm^{-1}. The respective band can be interpreted as an overlapping between the hydroxyl group of water and the other O-H containing functions. In the lower spectral region, between 1620-1630 cm^{-1} the low intensity peak can be attributed to the $\delta(H_2O)$. With the increase in temperature, the two O-H related bands tend to diminish in intensity with a total disappearance observed after 600°C.

Considering the just mentioned observations in the FTIR spectrum, it can be speculated that the noticed decrease in intensity of O-H vibrational modes is related to water and O-H containing moieties desorption from the NDs surface. Despite the fact that the spectra were recorded under the N_2 gas atmosphere, water molecules can still be tightly or loosely bound to the NDs surface [32].

Now, having a detailed look at the C-H band and its evolution, some explanations and links with the colloidal stability and concentration can be established. First, as mentioned before, the appearance of the C-H in the FTIR analysis is observed starting with 450°C. Secondly, it is observed that the highest concentration is obtained for the 500°C annealed sample and the suspension has good colloidal stability, thus it can be speculated that the "density" of C-H, C=O and other O containing groups on the surface are in such proportion that the colloidal behavior is optimized to be stable in water. For this sample, XPS analysis shows that the C-O content is at 22% while the C=O are at 2.6%.

Figure 18 depicts the C-H band evolution with increasing the temperature. It is seen that the shape and the wavenumber values differ between the several surface chemistries. Symmetric or asymmetric C-H bond vibrations have different wavenumber values and the respective assignments are summarized in Table 5 for samples annealed between 450°C and 800°C [11]. It is worth mentioning that annealing between 500°C and 700°C results in a more complex C-H band

with 3 assigned vibration modes. At 600°C, the asymmetric vibration mode of the CH_3 group is observed at 2950 cm^{-1}, compared to the rest of the samples that only show CH_2 stretching modes.

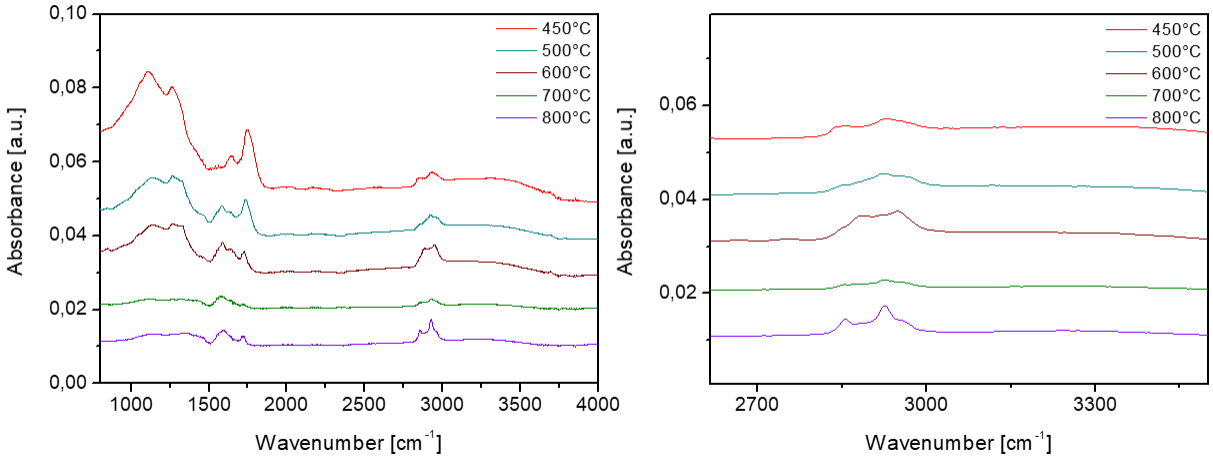

Figure 18. FTIR spectra of annealing treatments in the range 450°C-800°C showing the evolution of the C-H bands (right-hand graphic shows the spectral range characteristic to the C-H vibrations).

Table 5. Assignment of C-H bands.

Temperature [°C]	cm^{-1} value	Assignment	cm^{-1} value	Assignment	cm^{-1} value	Assignment
450	2930	CH_2 assym			2854	CH_2 sym
500	2968	Not assigned	2923	CH_2 assym	2852	CH_2 sym
600	2950	CH_3 assym	2921	CH_2 assym	2885	C-H stretching
700	2925	CH_2 assym	2885	C-H stretching	2855	CH_2 sym
800	2925	CH_2 assym			2854	CH_2 sym

The annealing treatments applied to the DNDs promote a shift of the zeta potential from negative values to positive values, going through a zone of no colloidal stability for the temperature range 300°C-400°C.

In literature and in the NDs community, the origin of the positive zeta potential is still under great debate, several possibilities exist. One explanation is the formation of sp^2 hybridized-carbon structure, either graphene shells or amorphous carbon, which can become protonated. The protonation occurs through the electron-donor-acceptor (EDA) complex. The sp^2 carbon structures contain π electron rich and oxygen depleted regions, which can absorb hydronium ions (H_3O^+), thus conferring a positive charge to the surface [33]. A second explanation was reported by Petit T. et al. [34] and explains that the surface transfer doping is the origin of the positive zeta potential through an accumulation of holes (h^+) at the surface. Looking at the FTIR spectra and XPS values, a decrease in the oxygen containing groups occurs simultaneously with the increase in sp^2 carbon content above 500°C. Between 500°C and 800°C, all samples have >40mV ζ-potential values, which can be related to the mentioned EDA complex. The suspensions follow the same stability

tendency for all atmospheres in which the sonication was carried out, implying that the accumulation of charges onto the NDs is independent of the sonication's chemical environment. Same observation stays valid for the average hydrodynamic diameter of the aggregates.

In the range of temperature 500-800°C the decrease in final concentration can be linked to the slight increase in C-C sp^2 content. This change in the C-C sp^2 influences the hydrophilic nature of the nanoparticles, so they become more hydrophobic. The reorganization of C atoms into sp^2-hybridized frameworks can be explained in the following manner: desorption of C-O and C=O groups (as shown by FTIR and XPS) leaves C atoms with dangling bonds. Thus, as thermal energy is transferred, the reactivity of these bonds leads to the formation of C-C sp^2 or C-H groups at the surface. Taking into consideration the final concentrations and the difference between the values of the suspensions obtained after the vacuum and hydrogenation treatments, a possible explanation could be the etching of sp^2 C-C by the H_2 gas.

4.2 HEALING OF DEFECTS

Detonation nanodiamonds contains defects, due to their synthesis method. This limits their use in several domains, namely in quantum and energy related application, where optical and semi-conducting properties of their diamond core need to be finely controlled. However, such defects (mainly carbon vacancies in the diamond lattice) can be repaired in some extend, by increasing the temperature. The relaxation of the structure will help to migrate the vacancies, which tend to reach the surface in the case of nanodiamonds. In this study, by the systematic XPS analysis of the annealed detonation nanodiamonds, we evidence this "healing" of the diamond core defects. Starting with a particle exhibiting a large component of defectuous C-C sp3, we were able to follow its decrease and the concomitant raise of the C-C sp3 diamond one. Such evolution of the C1s core level of detonation nanodiamonds has never been reported in the literature and constitutes a prime novelty.

4.3 GRAPHITIZATION KINETICS

Increasing the duration of the annealing treatments for the 1000°C and 1100°C temperatures did not affect the graphitization process significantly. Between 4h and 12h of annealing times at 1100°C, the sp^2 C-C content quantified by XPS does not vary crucially. On the other hand, the increase of 100°C proved to promote the reorganization of the carbon atoms into graphitic structures as observed in the diffraction patterns.

5. CONCLUSIONS AND PERSPECTIVES

The surface chemistry modifications, graphitization and colloidal stability of detonation nanodiamonds were studied upon applying thermal treatments ranging from 0°C to 1100°C. A thorough characterization of the untreated particles was also conducted. FTIR and XPS techniques were employed to assess the surface chemistry, while zeta potential measurements relate the colloidal stability. The untreated DNDs present a carboxylated surface and a high degree of defects near it and exhibit high colloidal stability (negative zeta potential in water). For the samples annealed between 200°C and 800°C, C-H formation starts at 450°C with a simultaneous reduction of COOH groups. Between 300°C and 400°C, the stability is lost and regained after 500°C with a high positive zeta potential value. Another observation include the increase in sp^3-hybrdized carbon and loss of defects, suggesting a "self-healing" process. Between 900°C and 1100°C the increase of sp^2-hybrdized carbon content is related to the reorganization of diamond into a π-conjugated framework.

Further investigations are necessary to complete this fundamental study. The perspectives of this research activity are centered on determination of origin of H leading to the formation of C-H bonds starting with 450°C. One approach would be the isotopic labelling with D_2 of the hydrogen containing functional groups. To confirm the quantification of defects in annealed NDs, EPR measurement are under progress on samples annealed from 200 and 900°C (collaboration with A. Taggliaferro, Torino). This technique allows the quantification of number of spins related to defects in nanodiamonds[18,19]. Then, the results of XPS regarding the formation of the sp^2-hybridized carbon can be completed by HR-TEM measurements, which would provide the base to calculate the thickness of the graphitic layer and visualize any changes of the diamonds core. Moreover, in addition to DLS measurements images obtained by cryo-TEM would be helpful in assessing the aggregates sizes and manner of organization.

REFERENCES

1. *Valery Yu. Dolmatov et al., Detonation nanodiamonds: new aspects in the theory and practice of synthesis, properties and applications, 2020 Russ. Chem. Rev. 89 1428.*
2. *R. Y. Yakovlev et al., Detonation nanodiamonds as promising drug carriers, Russ. J.Gen. Chem., 84, 379 – 390 (2012); doi: 10.1134/s1070363214020406.*
3. *A.V. Shvidchenko et al., Colloids of detonation nanodiamond particles for advanced applications, Advances in Colloid and Interface Science,Volume 268,2019, https://doi.org/10.1016/j.cis.2019.03.008.*
4. *A.M. Schrand et al., Nanodiamond particles: properties and perspectives for bioapplications, Crit. Rev. Solid State Mater. Sci., 34 (2009).*
5. *Ozawa, M. et al. Preparation and behavior of brownish, clear nanodiamond colloids. Adv. Mater. 19, 1201–1206 (2007).*
6. *Pentecost, A. et al., Deaggregation of nanodiamond powders using salt- and sugar-assisted milling. ACS Appl. Mater. Interfaces 2, 3289–3294 (2010).*
7. *Williams O.A. et al., Size-Dependent Reactivity of Diamond Nanoparticles, ACSNano 4 (2010) 4824-4830.*
8. *Bondar, V. S., Puzyr A. P. Nanodiamonds for biological investigations. Phys. Solid State 46, 716–719 (2004).*
9. *Arnault, J. C., Surface chemical modifications and surface reactivity of nanodiamonds hydrogenated by CVD plasma. Phys. Chem. Chem. Phys. 13, 11481–11487 (2011).*
10. *Mochalin, V.N. et al., The properties and applications of nanodiamonds, Nature nanotechnology, DOI: 10.1038/NNANO.2011.209 (2011).*
11. *Petit T., Puskar L., FTIR spectroscopy of nanodiamonds: Methods and interpretation, Diamond & Related Materials 89 (2018) 52–66.*
12. *Arnault J.C., X-ray Photoemission Spectroscopy applied to nanodiamonds: From surface chemistry to in situ reactivity, Diamond & Related Materials 84 (2018) 157-168.*
13. *Ozerin A.N. et al., X-ray Diffraction Study of the Structure of Detonation Nanodiamonds, Crystallography Reports 53 (2008), DOI:10.1134/S1063774508010070.*
14. *Yur'ev G.S., Dolmatov V. Yu., X-Ray Diffraction study of Detonation Nanodiamonds, Journal of Superhard Materials, 2010, Vol. 32, ISSN 10634576.*
15. *Van der Laan K.J. et al., Nanodiamonds for In Vivo Applications, Small 14 (2018), DOI: 10.1002/smll.201703838.*
16. *Aprà, P et al., Interaction of Nanodiamonds with Water: Impact of Surface Chemistry on Hydrophilicity, Aggregation and Electrical Properties. Nanomaterials 2021, 11, 2740. https://doi.org/10.3390/nano11102740.*
17. *Koscheev A. P., Gas Desorption from Detonation Nanodiamonds During Temperature Programmed Pyrolysis, Chapter 6 (2012), Pan Stanford Publishing Pte. Ltd., ISBN 978-981-4364-19-5.*
18. *Osipov V.Y. et al., Paramagnetic defects and exchange coupled spins in pristine ultrananocrystalline diamonds, Diam. Relat. Mater., 16 (2007).*
19. *Shames A.I. et al., Defects and impurities in nanodiamonds: EPR, NMR and TEM study, Jour. of Phys. and Chem. of Solids 63 (2002), PII: S0022-3697(02)00185-3.*
20. *Berdichevskiy G.M. et al., A comprehensive study of biocompatibility of detonation nanodiamonds, Journal of Molecular Liquids 332 (2021) https://doi.org/10.1016/j.molliq.2021.115763.*
21. *Arnault J-C. Surface modifications of nanodiamonds and current issues for their biomedical applications. Nianjun Y. Novel Aspects of Diamond - From Growth to Applications, 121 (Chapter 4), Springer Verlag, pp.85-122, 2015, Topics in Applied Physic,.*
22. *Petit T., Modifications de surface des nanodiamants: compréhension des mécanismes d'échange électroniques et mise en évidence d'un effet thérapeutique, Thèse de doctorat de l'école normale supérieure de Cachan, 2013.*
23. *Gibson N. et al., Colloidal stability of modified nanodiamond particles, Diamond & Related Materials 18 (2009) 620–626, doi:10.1016/j.diamond.2008.10.049.*
24. *Girard H. et al. Surface properties of hydrogenated nanodiamonds: a chemical investigation. Physical Chemistry Chemical Physics, Royal Society of Chemistry, 2011, 13 (24).*
25. *Kondo T. et al., Electrical conductivity of thermally hydrogenated nanodiamond powders, J. Appl. Phys. 113, 214307 (2013); https://doi.org/10.1063/1.4809549.*
26. *Duan X. et al., Nanodiamonds in sp2/sp3 configuration for radical to nonradical oxidation: Core-shell layer dependence, Applied Catalysis B: Environmental, Volume 222, 2018, 176-181, https://doi.org/10.1016/j.apcatb.2017.10.007.*
27. *Baer D.R. et al., Surface characterization of nanomaterials and nanoparticles: Important needs and challenging opportunities, Journal of Vacuum Science & Technology A 31, 050820 (2013), https://doi.org/10.1116/1.4818423.*
28. *Mead E.L. et al., The effect of ultrasound on water in the presence of dissolved gasses, Can J. Chem. 54, 1114 (1976).*
29. *Subpoena, Kruus P., Sonochemical formation of nitrate and nitrite in water, Ultrasonics Sonochemistry 7 (2000) 109–113, PII: S1350-4177 (99) 00043-7.*
30. *Hana Y. et al., Fluorescence indicative drop pH drop in sonication, Colloids and Surfaces A: Physicochem. Eng. Aspects 445 (2014) 30– 33, http://dx.doi.org/10.1016/j.colsurfa.2013.12.061.*
31. *Ducrozet, F et al., New Insights into the Reactivity of Detonation Nanodiamonds during the First Stages of Graphitization. Nanomaterials 2021, 11, 2671. https://doi.org/10.3390/nano11102671.*
32. *Koshcheev A.P. et al., The Chemistry of the Surface of Modified Detonation Nanodiamonds of Different Types, RUSSIAN JOURNAL OF PHYSICAL CHEMISTRY Vol. 82 No. 10 (2008), DOI:10.1134/S0036024408100129.*
33. *Ginés L. et al., Positive zeta potential of nanodiamonds, Nanoscale, 9, 12549 (2017), DOI: 10.1039/c7nr03200e.*
34. *Petit T. et al., Surface transfer doping can mediate both colloidal stability and self-assembly of nanodiamonds, Nanoscale, (2013), 5, 8958.*